# Single-Phase Phase-Locked Loop Based on Derivative Elements

Qingxin Guan, Yu Zhang, *Member, IEEE*, Yong Kang, and Josep M. Guerrero, *Fellow, IEEE*

***Abstract*—High-performance phase-locked loops (PLLs) are critical for power control in grid-connected systems. This paper presents a new method of designing a PLL for single-phase systems based on derivative elements (DEs). The quadrature signal generator (QSG) is constructed by two DEs with the same parameters. The PLL itself is realized by using the DE-based QSG. It avoids errors due to the overlap and accumulation that are present in PLLs based on integral elements, such as a PLL based on a second-order generalized integrator. Additionally, frequency feedback is not needed which allows the proposed PLL to achieve high performance when the grid frequency changes rapidly. This paper presents the model of the PLL and a theoretical performance analysis with respect to both the frequency-domain and time-domain behavior. The error arising from the discretization process is also compensated, ensuring this PLL method is suitable for implementation in a digital control system. Simulation and experimental results show that the proposed PLL achieves good performance in both harmonic rejection and dynamic response.**

***Index Terms*—Derivative element (DE), digital control, grid-connected system, phase-locked loop (PLL), single phase.**

## I. Introduction

PHASE-LOCKED LOOPS (PLLs) are critical for all types of grid-connected systems [1]–[4] and paralleled inverter systems [5], since they allow converters to exchange energy with the grid or realize the load sharing at high speed and with high accuracy. In grid-connected systems, the task of the PLL is to measure the frequency and phase angle of the fundamental components of grid voltage. PLL designs for single-phase grid-connected systems can be realized in both the frequency-domain and the time-domain.

The simplest PLL method detects the phase and frequency of the grid voltage by measuring the zero-crossing time [6]. However, this method has poor tracking performance because it only makes adjustments once per power cycle. Additionally, the accuracy is not guaranteed when the grid voltage is distorted.

PLL methods in the frequency-domain usually obtain the phase and frequency of the grid through a discrete-time Fourier transform [7], [8]. Although these algorithms achieve high precision, their heavy computational burden prevents them from achieving high dynamic performance.

PLL methods in the time-domain measure the instantaneous values of the grid voltage to detect the phase of the fundamental-frequency component [6]. Closed-loop feedback is used to synchronize the grid voltage signal with the application specific grid-connected system. The basic structure of the PLL feedback loop consists of three fundamental blocks: a phase detector (PD), a loop filter (LF), and a voltage-controlled oscillator. The performance of the PD is the most critical, as it is required to output the phase-angle error rapidly and accurately.

Conventional PDs used in three-phase systems are based on a synchronous-reference frame [9], while simple multipliers are typically used for PDs to build a power-based PLL in single-phase systems [6]. However, the output of a multiplier contains high-amplitude second-order harmonic, which greatly limits the bandwidth of the PLL and delays the response time [6]. To reduce the resulting ripple in the time domain, a first-order low-pass filter can be added as the LF [10]. The PD itself can also be improved, and Thacker *et al.* [11] proposed a mixer-type PD that can reduce the second harmonic by at least 50%. In [12], the variable time-delay PLL (VTD-PLL) is proposed, which is a fast digital PLL method based on a PD including a multiplier and a complex VTD algorithm. Additionally, using a PD based on in-quadrature signals can solve the second-harmonic problem completely [13], [14]. This type of system uses a quadrature signal generator (QSG) to generate two-phase orthogonal signals from the grid voltage, after which the Park transformation is used to obtain the phase error with high precision.

There are several ways of realizing a QSG [15], [16]. For example, a QSG can be realized by a $T/4$ transport delay buffer [17], with $T$ being the period of the grid voltage. However, this delay-based PLL fails to adapt to any rapid changes in the grid frequency. In [18], the QSG is based on an integrator. In [19]–[24], the QSG is based on the Hilbert transform, which involves the complex design of a finite impulse response filter and an infinite impulse response filter. In [23] and [24], the QSG is based on the inverse Park transformation. However, with this method, the QSG output is not in-quadrature unless the PLL is synchronized, which delays the transient process. Based on this kind of method, in [25], a PLL was proposed by using the dc-offset error compensation. It is also possible to use a parallel adaptive notch filter to estimate multiple frequencies as described in [26]–[29]; however, this type of system does not measure or synchronize the phase angle.

Manuscript received March 30, 2016; revised June 10, 2016; accepted August 8, 2016. Date of publication August 24, 2016; date of current version February 11, 2017. Recommended for publication by Associate Editor Dr. S. K. Panda.

Q. Guan, Y. Zhang, and Y. Kang are with the State Key Laboratory of Advanced Electromagnetic Engineering and Technology, Huazhong University of Science and Technology, Wuhan 430074, China (e-mail: guanqingxin@hust.edu.cn; zyu1126@mail.hust.edu.cn; ykang@mail.hust.edu.cn).

J. M. Guerrero is with the Institute of Energy Technology, Aalborg University, Aalborg 9200, Denmark (e-mail: joz@et.aau.dk).

Color versions of one or more of the figures in this paper are available online at http://ieeexplore.ieee.org.

Digital Object Identifier 10.1109/TPEL.2016.2602229

The current state-of-the-art in QSGs is based on a SOGI topology, which offers good performance [30]–[36]. In [30] and [31], multiple SOGIs are combined with a frequency-locked loop (FLL) to improve performance and obtain harmonic components. However, there are still potential issues with these architectures. In both of these works, the central frequency of the SOGI is supplied by the FLL, and fast changes in the central frequency can lead to the oscillation. Additionally, two integrator elements are used in each SOGI, which can be an issue in practical digital control systems. The problem of overlap and accumulation errors must be treated carefully in the microcontroller program or digital signal processor (DSP).

To overcome these issues, this paper presents a PLL based on derivative elements (DEs). With properly designed parameters, a DE-based QSG does not require a frequency feedback signal and can generate orthogonal signals without the risk of oscillations. Additionally, the problem of overlap and accumulation errors will no longer be an issue. This leads to potential improvements in the dynamic performance of the system while still guaranteeing the precision of the PLL.

The remainder of this paper is organized as follows. In Section II, the QSG based on a DE is described in detail. Section III presents the construction of the PLL based on derivate elements, along with the corresponding controller design. Section IV describes the discretization of the DE, and Sections V presents simulation and experimental results. Finally, Section VI concludes this paper.

## II. QSG Based on a DE

The transfer function of an ideal DE is given by

$$G_1(s) = s. \tag{1}$$

This generates a 90° phase shift, but also significantly amplifies the noise. Therefore, in a practical application, a filter also must be used. Combining the DE with a first-order low-pass filter (with time constant $T_1$) gives

$$G_2(s) = \frac{s}{T_1 s + 1}. \tag{2}$$

If the input signal of (2) is $v(t) = \sin(\omega t)$, the output will be

$$y(t) = \frac{\omega}{\sqrt{1+\omega^2 {T_1}^2}} \cdot \cos\left[\omega t - \arctan\left(\omega T_1\right)\right] - \frac{\omega e^{-t/T_1}}{1+\omega^2 {T_1}^2} \tag{3}$$

where the amplitude-frequency response is $m(\omega) = \omega/\sqrt{1+\omega^2 {T_1}^2}$. The derivative of $m(\omega)$ with respect to $\omega$ is

$$\dot{m}(\omega) = \frac{dm}{d\omega} = \left(1+\omega^2 {T_1}^2\right)^{-\frac{3}{2}}. \tag{4}$$

For all values of $\omega$, $\dot{m}(\omega) > 0$. This means $m(\omega)$ will increase monotonically with $\omega$, which means that higher order harmonics are amplified. This indicates that a first-order filter is not suitable for this application, and a second-order filter is necessary. Combining the DE with a second-order low-pass filter gives

$$G_3(s) = \frac{y_1(s)}{v(s)} = \frac{s}{T_1 \cdot T_2 s^2 + (T_1 + T_2)\, s + 1} \tag{5}$$

where $T_1$ and $T_2$ are the time constants of the second-order filter. If the input is $v = \sin(\omega t)$, the output from (5) is derived as

$$y_1(t) = \frac{\omega}{T_2 - T_1}\left(\frac{T_1 e^{-t/T_1}}{1+\omega^2 T_1^2} - \frac{T_2 e^{-t/T_2}}{1+\omega^2 T_2^2}\right) + \frac{\omega}{\sqrt{(1+\omega^2 T_1^2)\cdot(1+\omega^2 T_2^2)}} \cdot \cos\left(\omega t - \gamma\right). \tag{6}$$

When $t$ reaches infinity, the steady-state component of the output is

$$\begin{aligned} y_s(t) &= \lim_{t\to\infty} y_1(t) \\ &= \lim_{t\to\infty}\left[\frac{\omega}{T_2 - T_1}\left(\frac{T_1 e^{-t/T_1}}{1+\omega^2 T_1^2} - \frac{T_2 e^{-t/T_2}}{1+\omega^2 T_2^2}\right)\right] \\ &\quad + \lim_{t\to\infty}\left[\frac{\omega}{\sqrt{(1+\omega^2 T_1^2)\cdot(1+\omega^2 T_2^2)}} \cdot \cos\left(\omega t - \gamma\right)\right] \\ &= \frac{\omega}{\sqrt{(1+\omega^2 T_1^2)\cdot(1+\omega^2 T_2^2)}} \cdot \cos\left(\omega t - \gamma\right) \\ &= m(\omega) \cdot \cos\left(\omega t - \gamma\right) \end{aligned} \tag{7}$$

where $\gamma = \arctan[\frac{(T_1+T_2)\omega}{1-T_1 T_2 \omega^2}]$, and $m(\omega)$ is expressed as

$$m(\omega) = \frac{\omega}{\sqrt{(1+\omega^2 T_1^2)\cdot(1+\omega^2 T_2^2)}}. \tag{8}$$

The derivative of $m(\omega)$ with respect to $\omega$ is

$$\dot{m}(\omega) = \frac{dm}{d\omega} = \frac{1 - T_1^2 T_2^2 \omega^4}{[(1+\omega^2 T_1^2)\cdot(1+\omega^2 T_2^2)]^{\frac{3}{2}}}. \tag{9}$$

If we define $\omega_R = 1/\sqrt{T_1 \cdot T_2}$, we can see that for $\omega = \omega_R$, $\dot{m}(\omega) = 0$ and $m(\omega)$ reaches its maximum. For $\omega > \omega_R$, we can see that $\dot{m}(\omega) < 0$, which means higher order harmonics will be attenuated. Hence, if the frequency of the input signal fluctuates around $\omega_R$, the element will amplify the fundamental-frequency component while effectively attenuating higher order harmonics.

We can also write the transient component of (6) as

$$ex(t) = \frac{\omega}{T_2 - T_1}\left(\frac{T_1 e^{-t/T_1}}{1+\omega^2 T_1^2} - \frac{T_2 e^{-t/T_2}}{1+\omega^2 T_2^2}\right). \tag{10}$$

If we let $T_1 = T_2$ and calculate the limit as $T_2 \to T$, (10) becomes

$$\begin{aligned} ex(t) &= \lim_{T_2\to T}\left[\frac{\omega}{T_2 - T}\left(\frac{T e^{-t/T}}{1+\omega^2 T^2} - \frac{T_2 e^{-t/T_2}}{1+\omega^2 T_2^2}\right)\right] \\ &= \frac{\omega\left(1-\omega^2 T^2\right)e^{-t/T}}{\left(1+\omega^2 T^2\right)^2} + \frac{\omega t e^{-t/T}}{\left(1+\omega^2 T^2\right)T}. \end{aligned} \tag{11}$$

If the frequency of the input signal is exactly $\omega_R$, then $ex(t) = 0.5\,\omega_s^2 t e^{-\omega_s t}$. This shows that the transient process does not exhibit any overshoot or oscillations.

From $G_3(s)$, we can introduce another transfer function $G_4(s) = G_3(s)/s$ such that a pair of orthogonal signals is

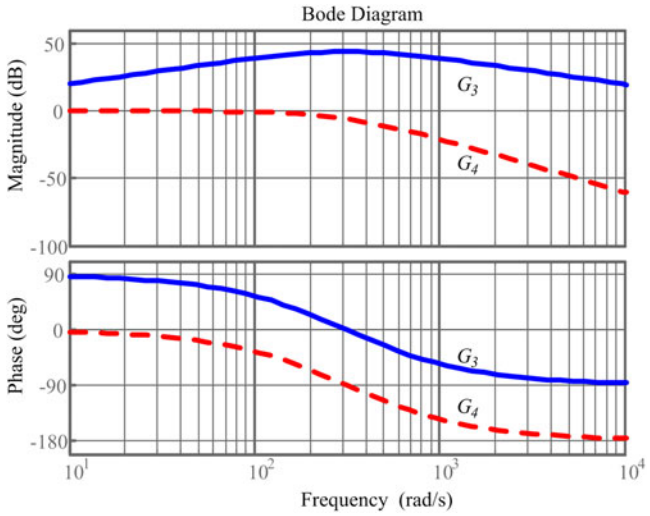


Fig. 1. Bode diagram of the proposed DE.

generated as follows:

$$\begin{bmatrix} y_1(s) \\ y_2(s) \end{bmatrix} = \begin{bmatrix} G_3(s) \\ G_4(s) \end{bmatrix} v(s) = \begin{bmatrix} \frac{s}{T_1 \cdot T_2 s^2 + (T_1+T_2)s+1} \\ \frac{1}{T_1 \cdot T_2 s^2 + (T_1+T_2)s+1} \end{bmatrix} v(s). \tag{12}$$

Equation (12) can be written as (13) when $T_1 = T_2 = T$

$$\begin{cases} G_3(s) = \frac{y_1}{v} = \frac{\omega_R^2 s}{s^2 + 2\omega_R s + \omega_R^2} \\ G_4(s) = \frac{y_2}{v} = \frac{\omega_R^2}{s^2 + 2\omega_R s + \omega_R^2} \end{cases}. \tag{13}$$

In practice, the frequency of the grid voltage is not a constant value, but will fluctuate around $\omega_R$. In order to examine the orthogonality of the output signals versus frequency, both of $G_3(s)$ and $G_4(s)$ are plotted in the Bode diagram of Fig. 1 by using MATLAB.

According to Fig. 1 and (13), we can observe that the proposed DE features the following characteristics.

1) The phase shifts between $y_1$ and $y_2$ is $\pi/2$ for all the values of $\omega$, which means it behaves as a QSG.
2) $G_3(s)$ acts as a bandpass filter with a central frequency of $\omega_R$, and $G_4(s)$ acts as a low-pass filter with a cut off frequency of $\omega_R$. Therefore, the DE can effectively track the signal near $\omega_R$, while simultaneously rejecting higher order harmonics.
3) The amplitude and frequency of the DE outputs are exclusively determined by the input, which is different than in the SOGI.
4) A phase error of $\gamma$ exists between $y_2$ and $v$, which can be written as

$$\gamma(\omega) = \arctan\left(\frac{2(\omega/\omega_R)}{1-(\omega/\omega_R)^2}\right). \tag{14}$$

Since the DE produces a pair of in-quadrature signals, it can be used to construct a high-precision PLL, which will be discussed in the next section.

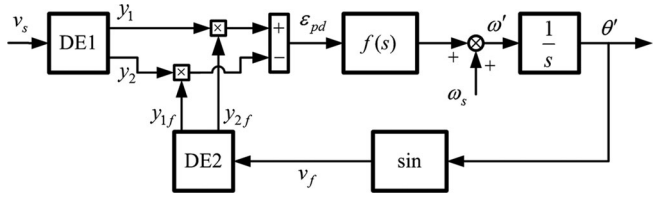


Fig. 2. Structure of a PLL based on DEs.

## III. PLL Based on DEs

### A. PLL Constructed by DEs

Fig. 2 shows the block diagram of a PLL constructed by using two DEs, i.e., DE1 and DE2. The $f(s)$ block represents the controller.

For an input of $v_s = \sin(\omega_s t + \theta_s)$, $\omega_R$ is set as $\omega_R = \omega_s$. According to (13), the signals generated by DE1 are

$$\begin{cases} y_1(t) = m(\omega_s) \cdot \cos(\omega_s t + \theta_s - \gamma_s) \\ y_2(t) = \frac{m(\omega_s)}{\omega_s} \cdot \sin(\omega_s t + \theta_s - \gamma_s) \end{cases} \tag{15}$$

where $\gamma_s = \gamma(\omega_s)$ is defined by (14). To compensate for a nonzero value of $\gamma_s$, another DE that has the same parameters as DE1 is added into the feedback loop. This is the element DE2 as shown in Fig. 2, and its outputs are

$$\begin{cases} y_{1f}(t) = m(\omega') \cdot \cos(\omega' t + \theta' - \gamma') \\ y_{2f}(t) = \frac{m(\omega')}{\omega'} \cdot \sin(\omega' t + \theta' - \gamma') \end{cases} \tag{16}$$

where $\gamma' = \gamma(\omega')$ is defined by (14).

Finally, the phase error signal $\varepsilon_{\rm pd}$ is calculated by the equation

$$\varepsilon_{\rm pd} = y_2 \cdot y_{1f} - y_1 \cdot y_{2f}. \tag{17}$$

When the PLL is nearly locked, i.e., $\omega' \approx \omega_s$, we obtain $\gamma' = \gamma(\omega') = \gamma(\omega_s) = \gamma_s$. In this case, $\varepsilon_{\rm pd}$ can be simplified as

$$\begin{aligned} \varepsilon_{\rm pd} &\approx m(\omega_s)\frac{m(\omega_s)}{\omega_s}\sin(\theta_s - \theta') \\ &\approx \frac{\omega_s}{4}\sin(\theta_s - \theta') \approx \frac{\omega_s}{4}(\theta_s - \theta'). \end{aligned} \tag{18}$$

As expected, $\varepsilon_{\rm pd}$ is independent of $\gamma_s$ and is proportional to the phase difference between the input signal $\theta_s$ and the output signal $\theta'$. Therefore, a PD has been realized. One thing to note is that the PD gain is $k_{\rm pd} = \omega_s/4$, which depends on the grid voltage frequency $\omega_s$. In a practical grid, the fluctuation of the grid voltage frequency is less than 5%. Under these circumstances, the PD gain will only vary slightly, and this will have almost no effect on the operation of the PLL. In addition, it is worth noting that the analysis done here is under the assumption that the amplitude of $v_s$ is 1. If the input signal is $v_s = V_m \sin(\omega_s t + \theta_s)$, the $\varepsilon_{\rm pd}$ must be divided by $V_m$.

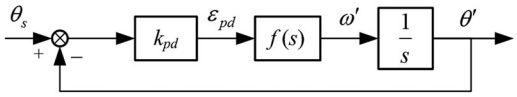


Fig. 3. Linear model of the DE-PLL.

### B. Parameter Design for the Proportional-Integral (PI) Controller

Fig. 3 shows the linearized model of the DE-PLL. A PI controller is chosen to implement the controller $f(s)$, which has the transfer function $f(s) = k_p + k_i/s$.

The closed-loop transfer function of the system in Fig. 3 is derived as

$$H_{\rm c}(s) = \frac{\theta'}{\theta_s} = \frac{k_p k_{\rm pd} s + k_i k_{\rm pd}}{s^2 + k_p k_{\rm pd} s + k_i k_{\rm pd}}. \tag{19}$$

This is a second-order system, and the undamped natural frequency $\omega_n$ and damping coefficient $\xi$ can be derived as

$$\begin{cases} \omega_n = \sqrt{k_i k_{\rm pd}} \\ \xi = \frac{k_p}{2}\sqrt{\frac{k_{\rm pd}}{k_i}} \end{cases}. \tag{20}$$

Using the standard representation of a second-order system, (19) can be rewritten as

$$H_{\rm c}(s) = \frac{2\xi\omega_n s + \omega_n^2}{s^2 + 2\xi\omega_n s + \omega_n^2}. \tag{21}$$

Equation (21) is a second-order system with one zero and two poles. In this system, as $\xi$ goes near zero, the poles approach the imaginary axis, and the response becomes oscillatory [32]. However, if $\xi > 1$, the speed of response becomes quite slow. The performance of second-order systems is normally measured by the step response, which settling time can be approximately calculated by (22) [6]

$$t_s \approx \frac{4.6}{\xi\omega_n} \tag{22}$$

and the overshoot can be calculated by

$$M_p = \frac{e^{-\xi(\pi + \arcsin\xi)/\sqrt{1-\xi^2}}}{\sqrt{1-\xi^2}} \times 100\%. \tag{23}$$

From (23) and (24), $\xi = 0.707$ is the best choice to achieve both a fast rise time and a low overshoot [38]. In order to guarantee the fast response of PLL, the settling time $t_s$ should be no more than 100 ms. Hence, the $\omega_n$ can be determined.

However, according to [6], $\omega_n$ is also related to the noise bandwidth of the PLL, which is

$$B_L = \int_0^\infty |H(j2\pi F)| \cdot dF \approx \frac{\omega_n}{8\xi}\left(1 + 4\xi^2\right). \tag{24}$$

The noise bandwidth is proportional to $\omega_n$. In order to filter harmonics effectively, the noise bandwidth is set as $B_L = 25 \times 2\pi$ rad/s. The value for $\omega_n$ can then be calculated as

$$\omega_n = \frac{8\xi}{1 + 4\xi^2} B_L = \frac{4\sqrt{2}}{9} B_L \approx 98.7307\,(\text{rad/s}). \tag{25}$$

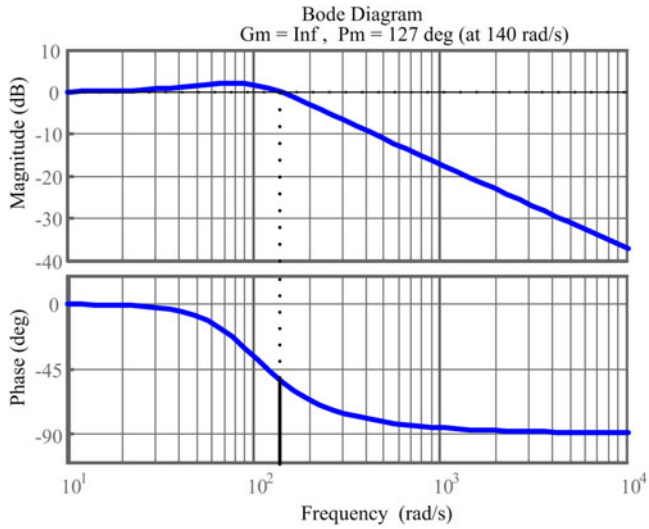


Fig. 4. Bode diagram of the DE-PLL.

For a grid with a frequency of 50% ± 5% Hz, $\omega_s = 100\pi$ rad/s and $k_{\rm pd} = \omega_s/4 \approx 78.54$. The parameters of the PI controller can be calculated as

$$\begin{cases} K_p = 2\xi\omega_n/k_{\rm pd} = 1.778 \\ K_i = \omega_n^2/k_{\rm pd} = 124.112 \end{cases}. \tag{26}$$

The resulting settling time can be calculated as $t_s \approx 0.0659$ (s), and the overshoot is $M_p \approx 2.79\%$ [37]. Fig. 4 shows the Bode diagram of the DE-PLL. This system is stable with a phase margin Pm = 127° and a gain margin Gm→∞.

## IV. Discretization of the PLL Based on DEs

### A. Discretization of the DE

By defining the sampling time as $T_s$ and writing $z = e^{j\omega T_s}$, the equations in (12) can be discretized by the backward differentiation formula [36]. The transfer functions in the discrete domain are given by

$$\begin{aligned} \begin{bmatrix} y_1(z) \\ y_2(z) \end{bmatrix} &= \begin{bmatrix} G_1(z) \\ G_2(z) \end{bmatrix} v(z) \\ &= \begin{bmatrix} \frac{{T_s}^2(z-1)}{T^2z^2 + 2T(T_s - T)z + (T_s - T)^2} \\ \frac{T_s}{T^2z^2 + 2T(T_s - T)z + (T_s - T)^2} \end{bmatrix} v(z). \end{aligned} \tag{27}$$

If $v(k) = \sin[\omega_s \cdot (kT_s) + \theta_s]$, the outputs can be derived from (27) as follows:

$$\begin{cases} y_1(k) = m(\omega_s) \cdot \cos\left[\omega_s \cdot (kT_s) + \theta_s - \gamma_s + \omega_s T_s/2\right] \\ y_2(k) = \frac{m(\omega_s)}{\omega_s} \cdot \sin\left[\omega_s \cdot (kT_s) + \theta_s - \gamma_s\right] \end{cases} \tag{28}$$

where $\gamma_s = \gamma(\omega_s)$ is defined by (14). The phase shift between $y_1(z)$ and $y_2(z)$ is no longer $\pi/2$, and in fact becomes

$$\varphi = (\pi + \omega_s T_s)/2. \tag{29}$$

This discretization process results in the phase error of $\omega_s T_s/2$. Therefore, a correction is needed to ensure the output signals are in-quadrature. Considering that

$$y_1(k-1) = m(\omega_s) \cdot \cos\left[\omega_s \cdot (kT_s) + \theta_s - \gamma_s - \omega_s T_s/2\right]. \tag{30}$$

A new intermediate variable can be introduced as

$$\begin{aligned} y_1^P(k) &= \frac{1}{2}\left[y_1(k-1) + y_1(k)\right] \\ &= m(\omega_s) \cdot \cos\left[\omega_s \cdot (kT_s) + \theta_s - \gamma_s\right] \cdot \cos(\omega_s T_s/2). \end{aligned} \tag{31}$$

For $T_s \le 2.8473 \times 10^{-4}$ (s), $\cos(\omega_s T_s/2) \ge 0.999$, i.e., $\cos(\omega_s T_s/2) \approx 1$, $y_1^P(k)$ can be written as

$$y_1^P(k) \approx m(\omega_s) \cos\left[\omega_s \cdot (kT_s) + \theta_s - \gamma_s\right]. \tag{32}$$

Therefore, the phase shift between $y_1^P(k)$ and $y_2(k)$ is $\pi/2$. $y_1^P(k)$ can, therefore, replace $y_1(k)$ as the output.

### B. Stability Analysis of the Closed-Loop System

The discrete transfer function of the closed-loop system is derived as

$$H_c(z) = \frac{k_{pd}k_p T_s z - k_{pd}k_p T_s + k_{pd}k_i T_s^2}{\left[z + \left(\frac{1}{2}k_{pd}k_p T_s - 1\right)\right]^2 + k_{pd}T_s^2\left(k_i - k_{pd}k_p^2/4\right)}. \tag{33}$$

This closed-loop system has the following two poles:

$$z_{1,2} = \left(1 - \frac{1}{2}k_{pd}k_p T_s\right) \pm jT_s\sqrt{k_{pd}\left(k_i - k_{pd}k_p^2/4\right)}. \tag{34}$$

For $k_{pd}k_p = 2\xi\omega_n$ and $k_{pd}k_i = \omega_n^2$, (34) can be written as

$$\begin{aligned} |z_{1,2}| &= \left|(1 - \xi\omega_n T_s) \pm j\sqrt{1-\xi^2}\omega_n T_s\right| \\ &= \sqrt{(1-\xi\omega_n T_s)^2 + (1-\xi^2)(\omega_n T_s)^2}. \end{aligned} \tag{35}$$

Since $\xi = 0.707$, $|z_{1,2}| = \sqrt{1 - 2\xi\omega_n T_s + {\omega_n}^2 {T_s}^2}$ which is located within the unit circle of the $z$ plane. Therefore, the stability of the system is guaranteed as long as the sampling time meets the condition of

$$T_s < 2\xi/\omega_n = 0.0143\ (\text{s}). \tag{36}$$

In practice, this condition is easily fulfilled.

## V. Simulation and Experimental Results

### A. Simulation Results

The proposed DE-PLL is simulated by using the S-function tools of MATLAB/Simulink. In order to simplify the simulation, the state equations of the DE were derived from (27) by defining $y_1$ and $v$ as state variables, which gives

$$\begin{bmatrix} \dot{y}_1 \\ \dot{y}_2 \end{bmatrix} = \begin{bmatrix} -\frac{1}{T^2} & -\frac{2}{T} \\ 0 & 1 \end{bmatrix} \begin{bmatrix} y_1 \\ y_2 \end{bmatrix} + \begin{bmatrix} \frac{1}{T^2} \\ 0 \end{bmatrix} v. \tag{37}$$

The grid voltage and frequency used for the simulations is 100 V/50 Hz. Scenarios of grid voltages with sag, phase jump, frequency step, frequency slope, and grid distortion are considered. As shown in [16], the SOGI-PLL shows satisfactory performance for it achieves a tradeoff between steady-state accuracy and dynamic response under a wide range of grid disturbance conditions. So that the SOGI-PLL was simulated as a comparison with its parameters designed in [33]. The input $v_s$, output phase $\theta'$, output frequency $\omega'$, and phase error $e = \theta_s - \theta'$ of DE-PLL and SOGI-PLL are plotted for each test case, respectively. In order to compare the performance of PLLs, the controller of DE-PLL has the same design parameters with SOGI-PLL, i.e., parameters used in all of the simulations were chosen as follows. An undamped natural frequency of $\omega_n = 98.7307$ rad/s, a damping coefficient of $\xi = 0.707$, and a sampling time of $T_s = 5 \times 10^{-5}$ s.

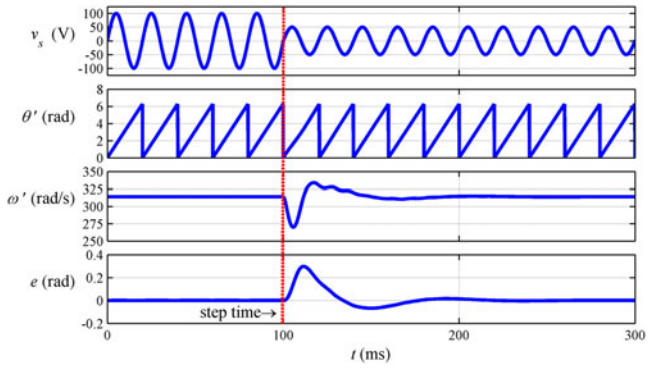


Fig. 5. Simulation results of DE-PLL for a 50% sag in the grid voltage (i.e., an amplitude step).

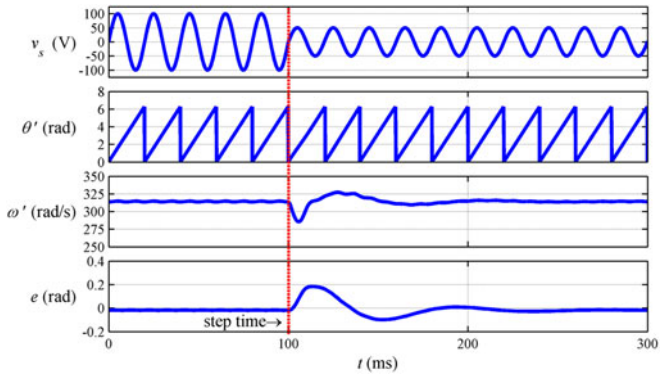


Fig. 6. Simulation results of SOGI-PLL for a 50% sag in the grid voltage (i.e., an amplitude step).

Figs. 5 and 6 show the behavior of the DE-PLL and SOGI-PLL under a grid voltage sag of 50% at $t = 0.1$ s. For the DE-PLL, the settling time is 0.0696 s and the overshoot of the output frequency is 14.05%. Whereas for the SOGI-PLL, the settling time is 0.0802 s and the overshoot is 9.14%. In this case, DE-PLL has higher overshoot of the output frequency signal and shorter settling time.

The simulation result for a 90° phase jump in the grid voltage is shown in Figs. 7 and 8 for the DE-PLL and SOGI-PLL respectively. For DE-PLL and SOGI-PLL, the overshoot of the

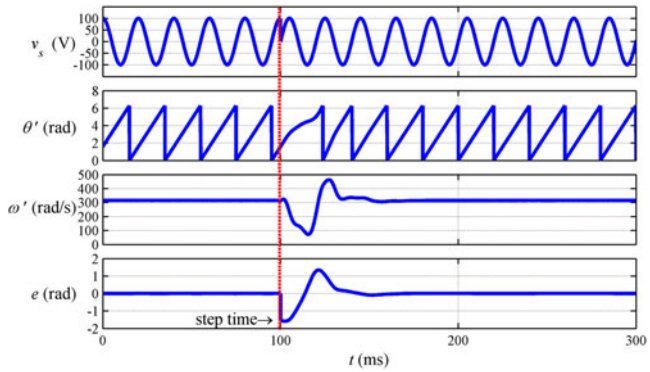


Fig. 7. Simulation results of DE-PLL for a phase step.

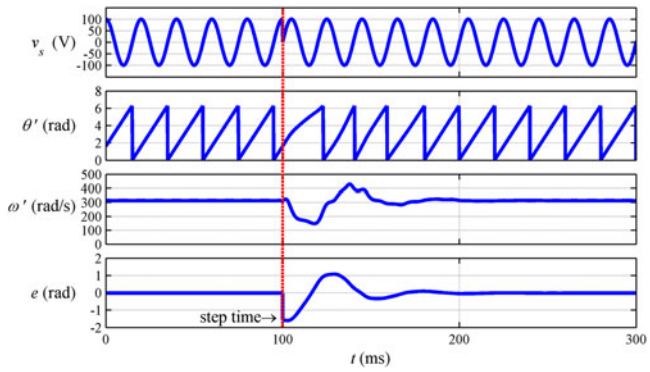


Fig. 8. Simulation results of SOGI-PLL for a phase step.

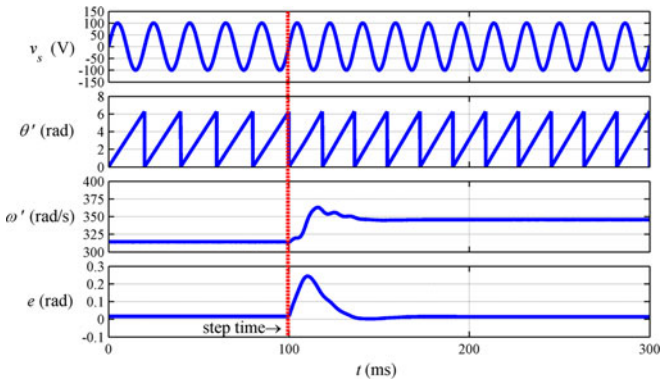


Fig. 9. Simulation results of DE-PLL for a frequency step.

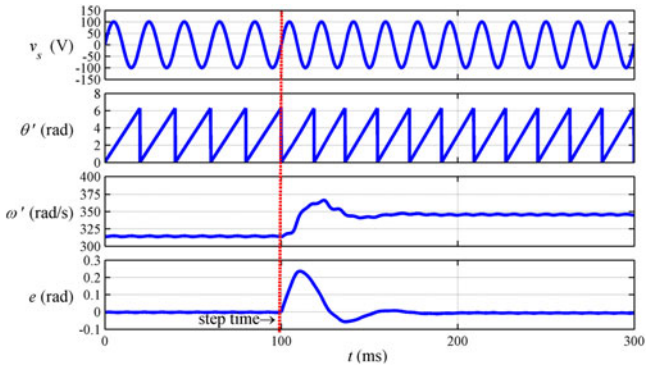


Fig. 10. Simulation results of SOGI -PLL for a frequency step.

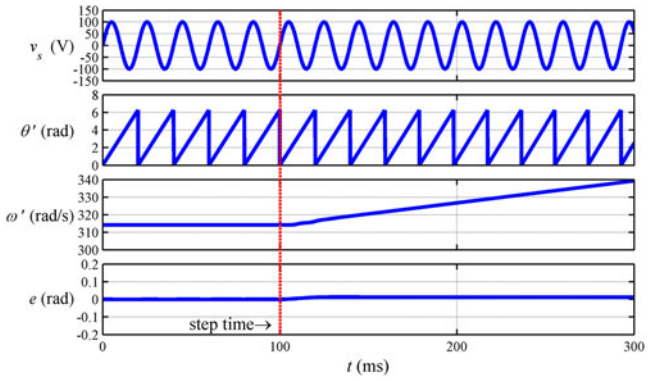


Fig. 11. Simulation results of DE-PLL for a frequency slope.

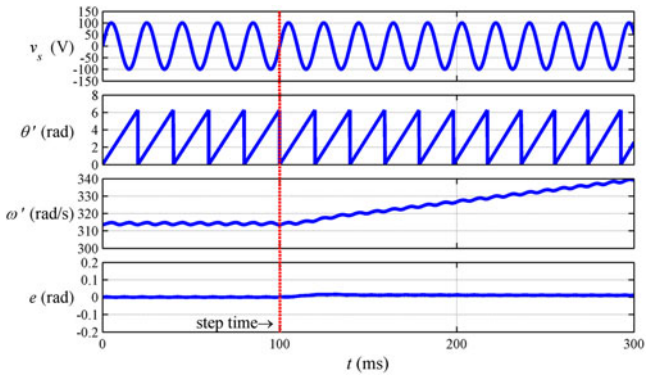


Fig. 12. Simulation results of SOGI -PLL for a frequency slope.

output frequency is 77.30% and 53.17% and the settling time is 0.0689 s and 0.1104 s separately.

Fig. 9 shows the simulation results of DE-PLL for a frequency step from 50 to 55 Hz in the grid voltage. The overshoot of the output frequency is 5% and the settling time is 0.0362 s. At the same time, Fig. 10 shows the simulation results of SOGI-PLL, in which the overshoot is 6% and the settling time is 0.0538 s. In Fig. 10, a small ripple is observed in the output frequency of SOGI-PLL, which is due to the feedback of frequency.

Figs. 11 and 12 show the simulation results for a frequency slope from 50 to 60 Hz in 0.2 s, which is started at $t = 0.1$ s. For both of the two PLLs, the output frequency signal follows the input frequency well with a small steady error. However, the output of DE-PLL are more smooth, while the SOGI-PLL output has a little ripple, which is due to the present of the frequency feedback.

Figs. 13 and 14 show the simulation results when the input grid voltage is distorted, causing harmonics to be injected at $t = 0.1$ s. The sinusoid of $\theta'$ ($\sin\theta'$) is also shown in this figure. The comparison of filtering performance between DE-PLL and SOGI-PLL with respect to the odd harmonics is shown in Table I. We can see that the output frequency signal of

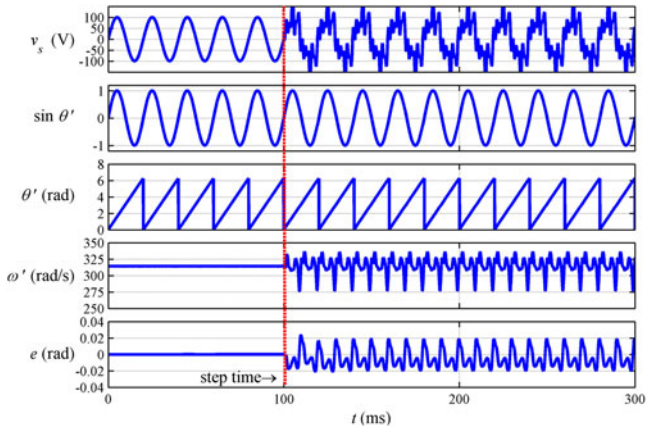


Fig. 13. Simulation results of DE-PLL in the presence of grid voltage distortion.

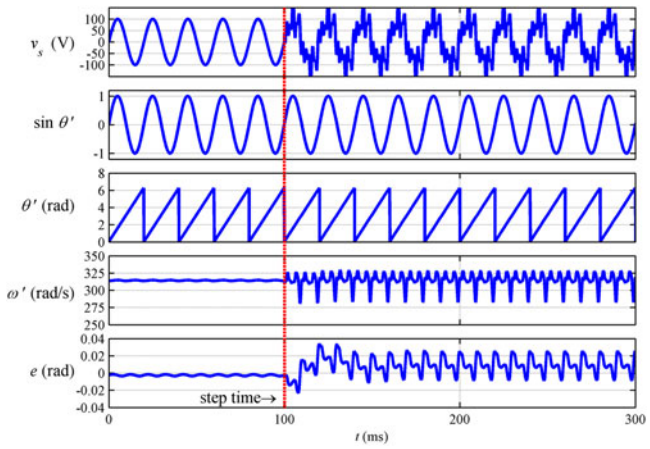


Fig. 14. Simulation results of SOGI-PLL in the presence of grid voltage distortion.

TABLE I
FILTERING PERFORMANCE OF THE DE-PLL AND SOGI-PLL

| Voltage component | THD (%) | 3rd harmonic (%) | 5th harmonic (%) | 7th harmonic (%) | 11th harmonic (%) |
|---|---|---|---|---|---|
| Input signal | 57.95 | 10 | 34 | 30 | 35 |
| Output of DE-PLL | 1.32 | 1.08 | 0.69 | 0.23 | 0.13 |
| Output of SOGI-PLL | 1.10 | 0.90 | 0.56 | 0.20 | 0.10 |

DE-PLL has no obvious oscillation in the presence of distortion and rapidly enters a state of stable operation. Whereas the SOGI-PLL has the same filter performance, but needs more time for the transient process.

As shown in the previous analysis, the DE-PLL has less frequency oscillatory than SOGI-PLL in the steady state. In cases of a grid voltage with sag and a phase jump, the settling time of DE-PLL is shorter than that of SOGI-PLL and larger overshoot. In case of a frequency step, DE-PLL has better performance than SOGI-PLL both in the settling time and overshoot. While the performance of these two PLLs is similar in case of a frequency slope and grid distortion.

In conclusion, DE-PLL presents faster response than the SOGI-PLL, especially in case of frequency changes. It also presents a less oscillating frequency signal in steady state.

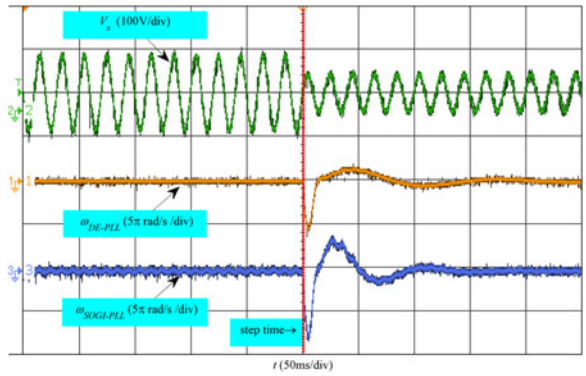


Fig. 15. Experimental results of DE-PLL and SOGI-PLL for a 50% sag in the grid voltage (i.e., an amplitude step).

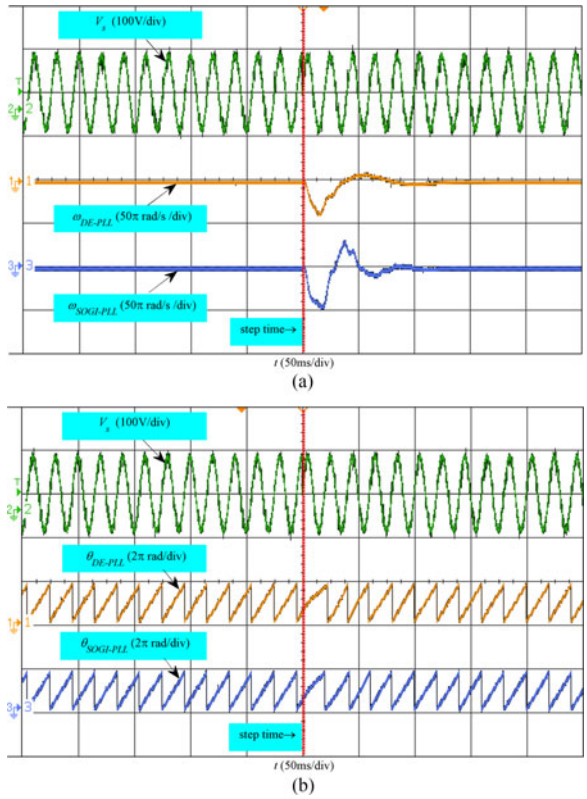


Fig. 16. Experimental results of DE-PLL and SOGI-PLL for a phase step. (a) Output frequency $\omega_{\mathrm{DE-PLL}}$ and $\omega_{\mathrm{SOGI-PLL}}$. (b) Output phase $\theta_{\mathrm{DE-PLL}}$ and $\theta_{\mathrm{SOGI-PLL}}$.

## B. Experimental Results

In order to verify the feasibility and effectiveness of this algorithm, the control system is implemented using a DSP chip from Texas Instruments (TMS320F28335). The output of DE-PLL and SOGI-PLL are observed using an oscilloscope through a DAC7724 chip.

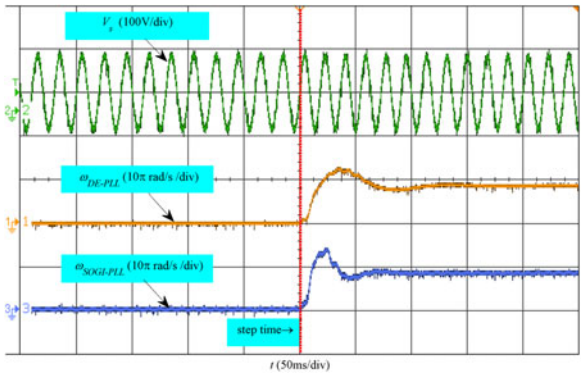


Fig. 17. Experimental results of DE-PLL and SOGI-PLL for a frequency step.

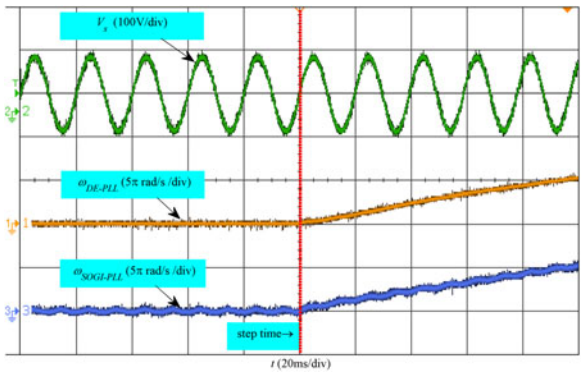


Fig. 18. Experimental results of DE-PLL and SOGI-PLL for a frequency slope.

Fig. 15 shows the behavior of the DE-PLL and SOGI-PLL under grid voltage sag of 50%. The settling time and overshoot of the DE-PLL are smaller than that of the SOGI-PLL. What is more, the frequency output of DE-PLL is smoother than that of the SOGI-PLL, which is consistent with the simulation results in Figs. 5 and 6.

Experimental results for a 90° phase jump in the grid voltage are shown in Fig. 16, in which the frequency output and phase output of two PLL were shown in Fig. 16(a) and 16(b) separately. The settling time of DE-PLL is roughly 40 ms and the settling time of SOGI-PLL is roughly 60 ms.

Fig. 17 shows the experimental results for a frequency step from 50 to 55 Hz, and the settling time of DE-PLL and SOGI-PLL are all roughly 60 ms.

Fig. 18 shows the experimental results of the response for a frequency slope. The experimental results show the same results as in the simulation. Notice that in this case, the output frequency exhibits no oscillation, while in case of the SOGI-PLL, output presents a considerable fluctuation.

Fig. 19 shows the experimental results when the input grid voltage is distorted by harmonic injection. The experimental results show a small settling time of about 30 ms.

The experimental results verify the excellent performance of the DE-PLL proposed in this paper, and show the possibility to implement this system easily. As shown in [39], the performance of PLL is important for the stability of grid-connected systems because their reference currents are obtained through the PLL.

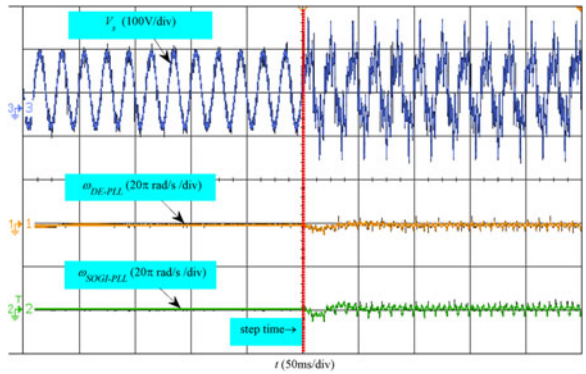


Fig. 19. Experimental results of DE-PLL and SOGI-PLL in the presence of grid voltage distortion.

For the same reason, the PLL is also critical for the paralleled inverter systems because the reference voltages are also obtained through the PLL [5]. The DE-PLL achieves high performance in obtaining high-accuracy phase and frequency signals from the input. The improved performance by DE-based PLL will significantly benefit the applications, such as grid-connected systems and paralleled inverter systems.

## VI. Conclusion

This paper presented a PLL based on DEs for use in systems connected to single-phase power grids. The DE has a simple structure, and it does not have the issues of overlap and accumulated error that are found in a traditional SOGI element. Its parameters are simply decided by the frequency of the grid voltage. The DE structure can effectively eliminate harmonics when configured to operate as a QSG, and its outputs track the input signal rapidly and accurately without overshoot or oscillation.

The PLL is constructed by using two DEs. Since feedback of the input or output frequencies to the DEs are not needed, a sudden change in input frequency does not lead to apparent oscillation. Choosing the parameters for the controller is a simple procedure, and the entire system can be efficiently implemented using a DSP. The performance of this system was compared with the SOGI-PLL through simulations and experiments, and the results showed that this system can be readily applied to practical power grid applications.

## References

[1] F. D. Freijedo, J. Doval-Gandoy, O. Lopez, P. Fernandez-Comesana, and C. Martinez-Penalver, "A signal-processing adaptive algorithm for selective current harmonic cancellation in active power filters," *IEEE Trans. Ind. Electron.*, vol. 56, no. 8, pp. 2829–2840, Aug. 2009.

[2] S. Golestan, M. Ramezani, and J. M. Guerrero, "DQ-frame cascaded delayed signal cancellation-based PLL: Analysis, design, and comparison with moving average filter-based PLL," *IEEE Trans. Power Electron.*, vol. 30, no. 3, pp. 1618–1632, Mar. 2015.

[3] T. V. Tran, T. W. Chun, H. H. Lee, H. G. Kim, and E. C. Nho, "PLL-based seamless transfer control between grid-connected and islanding modes in grid-connected inverters," *IEEE Trans. Power Electron.*, vol. 29, no. 10, pp. 5218–5228, Oct. 2014.

[4] K. M. S. Y. Konara, M. L. Kolhe, W. G. C. A. Sankalpa, A. R. Wimucthi, and D. D. M. Ranasinghe, "Integration of DC power source in micro-grid using VSI with PLL technique," in *Proc. 2015 Int. Conf. Smart Grid Clean Energy Technol.*, Offenburg, Germany, 2015, pp. 50–55.

[5] Y. Zhang, M. Yu, F. Liu, and Y. Kang, "Instantaneous current-sharing control strategy for parallel operation of UPS modules using virtual impedance," *IEEE Trans. Power Electron.*, vol. 28, no. 1, pp. 432–440, Jan. 2013.
[6] F. M. Gardner, *Phase Lock Techniques*. New York, NY, USA: Wiley, 1979.
[7] B. P. McGrath, D. G. Holmes and J. Galloway, "Improved power converter line synchronisation using an adaptive discrete Fourier transform (DFT)," in *Proc. IEEE 33rd Annu. Power Electron. Spec. Conf.*, Cairns, Australia, 2002, pp. 821–826.
[8] M. Karimi-Ghartemani, "Application of enhanced phase-locked loop system to the computation of synchro phasors," *IEEE Trans. Power Electron.*, vol. 28, no. 10, pp. 4550–4556, Oct. 2013.
[9] L. Feola, R. Langella, and A. Testa, "A unifying approach to single-phase synchronous reference frame PLLs," *IEEE Trans. Instrum. Meas.*, vol. 62, no. 9, pp. 2399–2409, Sep. 2013.
[10] S. Golestan, M. Monfared, F. D. Freijedo, and J. M. Guerrero, "Design and tuning of a modified power-based PLL for single-phase grid-connected power conditioning systems," *IEEE Trans. Power Electron.*, vol. 27, no. 8, pp. 3639–3650, Aug. 2012.
[11] T. Thacker, D. Boroyevich, R. Burgos, and F. Wang, "Phase-locked loop noise reduction via phase detector implementation for single-phase systems," *IEEE Trans. Ind. Electron.*, vol. 58, no. 6, pp. 2482–2490, Jun. 2011.
[12] A. Ozdemir and I. Yazici, "Fast and robust software-based digital phase locked loop for power electronics applications," *IET Gener. Transmiss. Distrib.*, vol. 7, no. 12, pp. 1435–1441, May 2013.
[13] C. Picardi, D. Sgro, and G. Gioffre, "A simple and low-cost PLL structure for single-phase grid-connected inverters," in *Proc. 2010 Int. Symp. Power Electron. Electr. Drives Autom. Motion*, Pisa, Italy, 2010, pp. 358–362.
[14] R. Teodorescu, M. Liserre, and P. Rodríguez, *Grid Converters for Photovoltaic and Wind Power Systems*. Chichester, U.K.: Wiley-IEEE Press, 2011.
[15] A. Nicastri and A. Nagliero, "Comparison and evaluation of the PLL techniques for the design of the grid-connected inverter systems," in *Proc. IEEE 2010 Int. Symp. Ind. Electron.*, Bari, Italy, 2010, pp. 3865–3870.
[16] Y. Han, M. Luo, X. Zhao, J. M. Guerrero, and L. Xu, "Comparative performance evaluation of orthogonal-signal-generators-based single-phase PLL algorithms—A Survey," *IEEE Trans. Power Electron.*, vol. 31, no. 5, pp. 3932–3944, May 2016.
[17] R. E. Best, *Phase-Locked Loops: Design, Simulation, and Applications*, 5th ed. New York, NY, USA: McGraw-Hill, 2003.
[18] F. A. Ramirez, and M. A. Arjona, "Development of a grid-connected wind generation system with a modified PLL structure," *IEEE Trans. Sustainable Energy*, vol. 3, no. 3, pp. 474–481, Jul. 2012.
[19] M. Saitou, N. Matsui, and T. Shimizu, "A control strategy of single-phase active filter using a novel d-q transformation," in *Proc. 38th Ind. Appl. Conf. Annu. Meet.*, 2003, pp. 1222–1227.
[20] H. S. Kim, M. H. Ryu, J-.W. Baek, and J. H. Jung, "High-efficiency isolated bidirectional AC–DC converter for a DC distribution system," *IEEE Trans. Power Electron.*, vol. 28, no. 4, pp. 1642–1654, Apr. 2013.
[21] C. M. Rader and L. B. Jackson, "Approximating noncausal IIR digital filters having arbitrary poles, including new Hilbert transformer designs, via forward/backward block recursion," *IEEE Trans. Circuits Syst. I, Reg. Papers*, vol. 53, no. 12, pp. 2779–2787, Dec. 2006.
[22] F. Gonzalez-Espin, E. Figueres, and G. Garcera, "An adaptive synchronous-reference-frame phase-locked loop for power quality improvement in a polluted utility grid," *IEEE Trans. Ind. Electron.*, vol. 59, no. 6, pp. 2718–2731, Jun. 2012.
[23] S. M. Silva, B. M. Lopes, B. J. C. Filho, R. P. Campana, and W. C. Bosventura, "Performance evaluation of PLL algorithms for single-phase grid-connected systems," in *Proc. 39th Ind. Appl. Conf. Annu. Meet.*, Seattle, WA, USA, 2004, pp. 2259–2263.
[24] Z. Wang, S. Fan, Y. Zheng, and M. Cheng, "Control of a six-switch inverter based single-phase grid-connected PV generation system with inverse Park transform PLL," in *Proc. IEEE 2012 Int. Symp. Ind. Electron.*, Hangzhou, China, 2012, pp. 258–263.
[25] S. H. Hwang, L. Liu, and H. Li, "DC offset error compensation for synchronous reference frame PLL in single-phase grid-connected converters," *IEEE Trans. Power Electron.*, vol. 27, no. 8, pp. 3467–3471, Aug. 2012.
[26] D. Yazdani *et al.*, "A nonlinear adaptive synchronization technique for grid-connected distributed energy sources," *IEEE Trans. Power Electron.*, vol. 23, no. 4, pp. 2181–2186, Jul. 2008.
[27] M. Karimi-Ghartemani, A. R. Bakhshai, and M. Mojiri, "Estimation of power system frequency using adaptive notch filter," in *Proc. IEEE Instrum. Meas. Technol. Conf.*, Ottawa, Canada, 2005, pp. 1494–1497.
[28] M. Mojiri, M. Karimi-Ghartemani, and A. Bakhshai, "Time-domain signal analysis using adaptive notch filter," *IEEE Trans. Signal Process.*, vol. 55, no. 1, pp. 85–93, Jan. 2007.
[29] L. Wang, D. Zhang, C. Zhang, and Z. Lu, "A high performance PLL for polluted utility grid based on cascade adaptive notch filters," in *Proc. 2012 7th Int. Power Electron. Motion Control Conf.*, Harbin, China, 2012, pp. 615–619.
[30] P. Rodríguez, A. Luna, I. Candela, R. Teodorescu, and F. P. Blaabjerg, "Grid synchronization of power converters using multiple second order generalized integrators," in *Proc. IEEE 34th Annu. Conf. Ind. Electron*, Orlando, FL, USA, 2008, pp. 755–760.
[31] P. Rodríguez, A. Luna, I. Candela, R. Mujal, R. Teodorescu, and F. Blaabjerg, "Multiresonant frequency-locked loop for grid synchronization of power converters under distorted grid conditions," *IEEE Trans. Ind. Electron.*, vol. 58, no. 1, pp. 127–138, Jan. 2011.
[32] R. C. Dorf and R. H. Bishop, *Modern Control Systems*, 12th ed. New York, NY, USA: Pearson Education, Inc. 2011.
[33] P. Rodríguez *et al.*, "New positive-sequence voltage detector for grid synchronization of power converters under faulty grid conditions," in *Proc. IEEE 37th Annu. Power Electron. Spec. Conf.*, Jeju, South Korea, 2006, pp. 1–7.
[34] M. Ciobotaru, R. Teodorescu, and F. Blaabjerg, "A new single-phase PLL structure based on second order generalized integrator," in *Proc. IEEE 37th Annu. Power Electron. Spec. Conf.*, Jeju, South Korea, 2006, pp. 1–6.
[35] S. Golestan, M. Monfared, F. D. Freijedo, and J. M. Guerrero, "Dynamics assessment of advanced single-phase PLL structures," *IEEE Trans. Ind. Electron.*, vol. 60, no. 6, pp. 2167–2177, Jun. 2013.
[36] Y. Yang, F. Blaabjerg, and Z. Zou, "Benchmarking of grid fault modes in single-phase grid-connected photovoltaic systems," *IEEE Trans. Ind. Appl.*, vol. 49, no. 5, pp. 2167–2176, Sep. 2013.
[37] Y. Wang and Y. Li, "Grid synchronization PLL based on cascaded delayed signal cancellation," *IEEE Trans. Power Electron.*, vol. 26, no. 7, pp. 1987–1997, Jul. 2011.
[38] E. Rogers, K. Galkowski, and D. H. Owens, *Control Systems Theory and Applications for Linear Repetitive Processes*. Berlin, Germany: Springer, 2007.
[39] C. Zhang, X. Wang, F. Blaabjerg, W. Wang, and C. Liu, "The influence of phase-locked loop on the stability of single-phase grid-connected inverter," in *Proc. IEEE 2015 Energy Convers. Congr. Expo.*, Montreal, Canada, 2015, pp. 4737–4744.

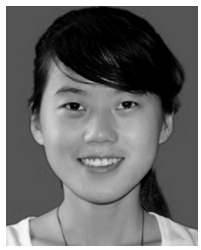

**Qingxin Guan** was born in Jilin Province, China. She received the B.S. degree in electrical engineering and automation from Harbin Institute of Technology, Harbin, China, in 2013. She is currently working toward the Ph.D. degree in electrical engineering in the School of Electrical and Electronic Engineering, Huazhong University of Science and Technology.

Her research interest includes high-efficiency inverter power supply.

**Yu Zhang** (M'11) was born in Jiangsu Province, China. He received the B.E., M.E., and Ph.D. degrees in electrical engineering from Huazhong University of Science and Technology (HUST), Wuhan, China, in 1992, 1995, and 2005, respectively.

From 1995 to 2002, he was an Engineer with power supply applications, Wuhan Telecommunication Company. He is currently an Associate Professor with the School of Electrical and Electronic Engineering, HUST, where he teaches power electronics. He has developed several power systems, such as modular UPS. His research interests include power electronics modeling and control, parallel UPSs, and renewable energy generation.

Dr. Zhang is currently the Member of the UPS Standard Committee of China. He has received four Scientific and Technology Awards.

**Yong Kang** was born in Hubei Province, China. He received the B.E., M.E., and Ph.D. degrees from Huazhong University of Science and Technology (HUST), Wuhan, China, in 1988, 1991, and 1994, respectively.

In 1994, he joined HUST as a Lecturer and was promoted to an Associate Professor in 1996 and to a Full Professor in 1998. He is currently the Vice Chairman of the China UPS Standard Committee and the Head of the School of Electrical and Electronic Engineering, HUST. He is the Author of more than 200 technical papers and the Associate Editor of the *Journal of Power Electronics*. His research interests include power electronic converters, ac drivers, renewable energy generation, and EMC techniques.

**Josep M. Guerrero** (S'01–M'04–SM'08–FM'15) received the B.S. degree in telecommunications engineering, the M.S. degree in electronics engineering, and the Ph.D. degree in power electronics from the Technical University of Catalonia, Barcelona, Spain, in 1997, 2000, and 2003, respectively.

Since 2011, he has been a Full Professor in the Department of Energy Technology, Aalborg University, Aalborg, Denmark, where he is responsible for the Microgrid Research Program; since 2012, he has been a Guest Professor with the Chinese Academy of Science, Beijing, China, and the Nanjing University of Aeronautics and Astronautics, Nanjing, China; since 2014, he has been the Chair Professor with Shandong University, Shandong, China; and since 2015, he has been a Distinguished Guest Professor with Hunan University, Hunan, China. His research interests include different microgrid aspects, including power electronics, distributed energy storage systems, hierarchical and cooperative controls, energy management systems, and optimization of microgrids and islanded minigrids.